Spanish Journal of Agricultural Research
17 (2), e0203, 11 pages (2019)
eISSN: 2171-9292
https://doi.org/10.5424/sjar/2019172-14449
Instituto Nacional de Investigación y Tecnología Agraria y Alimentaria, O.A, M.P. (INIA)

RESEARCH ARTICLE

OPEN ACCESS

Parameter optimization of winnowing equipment for machine-harvested *Lycium barbarum* L.

Jian Zhao[1], Adilet Sugirbay[1,2], Fanyi Liu[3], Yun Chen[1], Guangrui Hu[1], Enyu Zhang[1] and Jun Chen[1]

[1]Northwest A&F Univ., College of Mechan. & Electron. Eng., Yangling, 712100 Shaanxi, China. [2]S. Seifullin Kazakh Agro Tech. Univ., Techn. Fac., Astana 010000, Kazakhstan. [3]SouthWest Univ., College of Eng. & Technol., Beibei, 400715 Chongqing, China.

Abstract

To accurately and efficiently remove unripe fruit, flowers, leaves, and other impurities in machine-harvested *Lycium barbarum* L., winnowing equipment for machine-harvested *L. barbarum* based on the principle that different materials have different flight coefficients was designed. To optimize the structure and working parameters of winnowing equipment, this study adopted the free flow resistance model to establish a horizontal airflow model based on C++ in Microsoft Visual Studio. A discrete element method (DEM) simulation of ripe fruit in the horizontal airflow was performed using EDEM software. Results showed that the optimal parameters included an airflow speed of 5-6 m/s, input conveyor speed of 0.4-0.6 m/s, and input-output conveyor distance of 260-270 mm. We used three factors and three levels in a quadratic orthogonal rotation design to establish mathematical models regarding the rate of impurity change and the clearance rate of ripe fruit based on the airflow speed, input conveyor speed, and input-output conveyor distance. We also analyzed the effects of all factors on the rate of impurity change and the clearance rate of ripe fruit. The optimal parameter combination was an airflow speed of 5.52 m/s, input conveyor speed of 0.5 m/s, and input-output conveyor distance of 265.04 mm. The field experiment showed that the rate of impurity change and the clearance rate of ripe fruit were 89.74% and 8.71%, respectively. Findings provide a design basis for future research on winnowing equipment for machine-harvested *L. barbarum*.

Additional keywords: flight coefficient; free flow resistance model; discrete element method; response surface methodology.

Abbreviations used: DEM (discrete element method); DF (degree of freedom).

Authors' contributions: Conceived and designed the experiments: JZ, AS and JC. Performed the experiments: JZ, YC, GH, and EZ. Analyzed the data: JZ and FL. Wrote the paper: JZ, AS, and JC. All authors read and approved the final manuscript.

Citation: Zhao, J.; Sugirbay, A.; Liu, F. Y.; Chen, Y.; Hu, G. G.; Zhang, E.; Chen, J. (2019). Parameter optimization of winnowing equipment for machine-harvested *Lycium barbarum*. Spanish Journal of Agricultural Research, Volume 17, Issue 2, e0203. https://doi.org/10.5424/sjar/2019172-14449

Received: 27 Dec 2018. **Accepted:** 01 Jul 2019.

Funding: National Key Research and Development Program of China (2017YFD0700402, 2018YFD0701102); Key Research and Development Program of the Ningxia Hui Autonomous Region (nxzdkjxm2016-04-02).

Competing interests: The authors have declared that no competing interests exist.

Correspondence should be addressed to Jun Chen: chenjun_jdxy@nwsuaf.edu.cn

Introduction

Lycium barbarum L. is a solanaceous *Lycium* shrub (Xu *et al.*, 2018). Its ripe fruit contains health-promoting bioactive components such as *L. barbarum* polysaccharides (Amagase & Farnsworth, 2011). The polysaccharides have demonstrated its effects on the improvement of renal function and the alleviation of inflammatory reaction (Zhao *et al.*, 2016). For centuries, mechanized harvesting of *L. barbarum* has been challenging. Therefore, the fruit are harvested manually, which involves low efficiency and high cost (Zhang *et al.*, 2015; Xu *et al.*, 2018). With the continuous expansion of *L. barbarum* acreage, labor for fruit harvesting has become increasingly scarce, leading to more *L. barbarum* harvesting machines to be developed and used (So, 2001, 2003; Zhou & He, 2010; Zhang *et al.*, 2015; He *et al.*, 2017; Wang, 2018; Wang *et al.*, 2018; Xu *et al.*, 2018; Zhang *et al.*, 2018a,b; Chen *et al.*, 2019; Zhao *et al.*, 2019b). However, many impurities such as unripe fruit, flowers, and leaves in machine-harvested *L. barbarum* seriously affect subsequent drying, storage, and other processing procedures (Zhang *et al.*, 2015; Wang, 2018; Xu *et al.*, 2018; Zhang *et al.*, 2018b; Chen *et al.*, 2019; Zhao *et al.*, 2019b). Therefore, it is important to develop accurate and efficient winnowing equipment to remove impurities such as unripe fruit, flowers, and leaves in machine-harvested *L. barbarum*.

Winnowing equipment for machine-harvested *L. barbarum* was designed based on the principle that

different materials have different flight coefficients. Using a discrete element method (DEM) simulation and the field experiment, the structure and working parameters of winnowing equipment were optimized. The results provide a design basis for future research and development of winnowing equipment for machine-harvested *L. barbarum*.

Material and methods

Structure and operating principle of winnowing equipment

Structure of winnowing equipment

Winnowing equipment for machine-harvested *L. barbarum* is shown in Fig. 1. The equipment consisted of a mechanical transmission system, winnowing system, and control system. The mechanical transmission system consisted of an input conveyor, output conveyor, electric motors, and drive systems; the winnowing system consisted of a fan, electronic speed regulator, and lithium battery; and the control system consisted of a controller, electronic speed governors, and relays.

Operating principle of winnowing equipment

As shown in Fig. 2, ripe fruit in the horizontal airflow was subjected to three forces: gravity G, horizontal airflow force P, and buoyancy F_B. Because the buoyancy has a slight influence on the movement of ripe fruit in the horizontal airflow compared with the gravity and horizontal airflow force, it can be ignored (Liu, 2013). After simplification, the angle α between the resultant force of gravity and horizontal airflow force and the gravity can be obtained. When ripe fruit entered the horizontal airflow, its movement under the resultant force was parabolic and the distance of the movement of ripe fruit was related to the angle α (Liu, 2013). The larger the angle α, the farther the distance; the smaller the angle α, the closer the distance. The tangent of angle α can be expressed as the ratio of P to G and is calculated as follows (Liu, 2013).

$$\tan\alpha = \frac{P}{G} = \frac{K\rho B\left(V_a - V_x\right)^2}{G} \quad [1]$$

where P is the horizontal airflow force, N; G is the gravity of ripe fruit, N; K is the resistance coefficient, which is related to the shape and surface characteristics of ripe fruit; ρ is the density of horizontal airflow, kg/m^3; B is the windward area of ripe fruit in the horizontal airflow, m^2; V_a is the velocity of horizontal airflow, m/s; and V_x is the initial velocity of ripe fruit entering the horizontal airflow, m/s.

The tangent of angle α is called the flight coefficient and is the characteristic value of the aerodynamic property of ripe fruit in the horizontal airflow (Liu, 2013). As shown in Table 1, because flying coefficients of different materials in the same horizontal airflow are different (Liu, 2013), the horizontal airflow can be used to remove impurities such as unripe fruit, flowers, and leaves in machine-harvested *L. barbarum*.

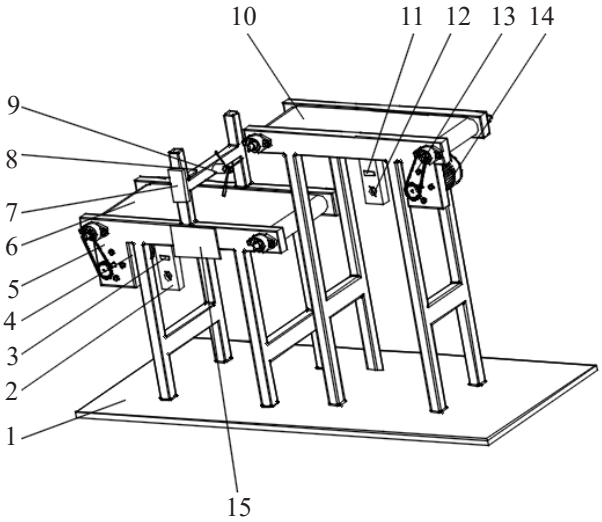

Figure 1. Winnowing equipment for machine-harvested *Lycium barbarum*. 1, frame; 2, electronic speed governor of the output conveyor; 3, relay of the output conveyor; 4, electric motor of the output conveyor; 5, drive system of the output conveyor; 6, output conveyor; 7, lithium battery; 8, electronic speed regulator; 9, fan; 10, input conveyor; 11, relay of the input conveyor; 12, electronic speed governor of the input conveyor; 13, drive system of the input conveyor; 14, electric motor of the input conveyor; 15, controller.

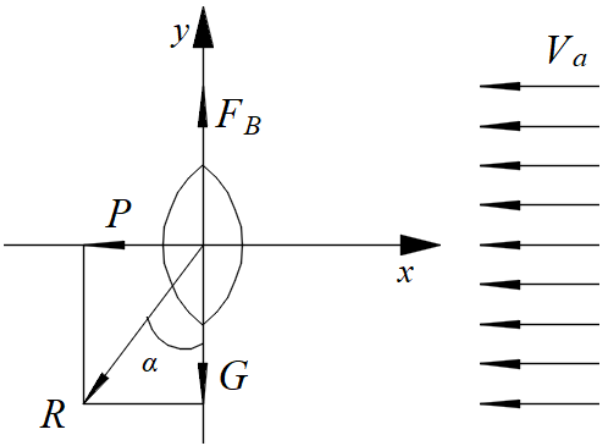

Figure 2. Force analysis of ripe fruit in the horizontal airflow. R is the resultant force of gravity and horizontal airflow force, N.

Table 1. Shape and mechanics parameters of materials.

Material	Mass (g)	Density (kg/m^3)	Elastic modulus (MPa)	Poisson's ratio	Major axis (mm)	Minor axis (mm)	Thickness (mm)
Ripe fruit[a]	1.343	895	0.05	0.39	16.54	10.51	7.86
Unripe fruit	0.298	1108	2.83	0.41	12.05	5.04	4.72
Flower	0.024	-	-	-	-	-	-
Leaf	0.274	-	-	-	-	-	-
Input conveyor[b]	-	1130	2320	0.34	-	-	-

[a]Data from Zhao *et al.* (2019a). [b]Data from Baidu (2015).

Design of key systems

Mechanical transmission system

Because machine-harvested *L. barbarum* was transported on the conveyors and we needed to adjust the input conveyor speed, the design of the input conveyor and output conveyor was highly important. The two transmission shafts were parallel, the rotation direction of the two transmission shafts was the same, and the input conveyor speed was ≤ 20 m/s; thus, the open drive mode can be selected (Qiu, 2011). As the transmission power W was<500 kW, the belt of the input conveyor and output conveyor was made of anti-static flat belt (Qiu, 2011). The design equations [2-8] were referred to this book (Qiu, 2011). The effective tensile force was obtained as follows:

$$F = F_1 - F_2 = \frac{1000W}{X_2} \quad [2]$$

where F is the effective tensile force of the input conveyor, N; F_1 is the tight-side tensile force of the input conveyor, N; F_2 is the slack-side tensile force of the input conveyor, N; W is the nominal transmission power of the input conveyor, kW; and X_2 is the input conveyor speed, m/s.

The relation equation between the tight-side tensile force of the input conveyor and the slack-side tensile force of the input conveyor can be obtained as follows:

$$\frac{F_1 - qX_2^2}{F_2 - qX_2^2} = e^{\mu\lambda} \quad [3]$$

where q is the mass of a meter length belt of the input conveyor, kg/m; e is the Napierian base; μ is the friction coefficient between the input conveyor and its belt wheel; and λ is the cornerite between the input conveyor and its belt wheel, (°).

Because the input conveyor speed was<10 m/s, the centrifugal force can be ignored (Qiu, 2011). Because $\lambda=\pi$, $\mu \approx 0.3$. Therefore, the calculated transmission power W_c can be obtained as follows:

$$W_c = K_A W \quad [4]$$

where W_c is the calculated transmission power of the input conveyor, kW; and K_A is the working condition coefficient.

Therefore, the equations of the diameter of the driving wheel of the input conveyor D_1, diameter of the driven wheel of the input conveyor D_2, and center distance of the input conveyor s are as follows:

$$D_1 = (1100 - 1350)\left(\frac{W_c}{m_1}\right)^{\frac{1}{3}} \quad [5]$$

$$D_2 = iD_1(1-\varepsilon) \quad [6]$$

$$1.5(D_1 + D_2) \le s \le 5(D_1 + D_2) \quad [7]$$

where D_1 is the diameter of the driving wheel of the input conveyor, mm; m_1 is the revolving speed of the driving wheel of the input conveyor, r/min; D_2 is the diameter of the driven wheel of the input conveyor, mm; i is the transmission ratio of the input conveyor; ε is the sliding rate of the input conveyor, %; and s is the center distance of the input conveyor, mm.

The design of the output conveyor was as outlined above. After calculation, the design parameters of conveyors are listed in Table 2.

According to the nominal transmission power, the electric motors adopted alternating current electric motors (type: 5GN30KB; rated power: 60W; reduction ratio: 1:30; manufactured by Guangdong Shengkai Motor Manufacturing Co., Ltd., China). The input conveyor and output conveyor can be driven to rotate by the toothed chain. The toothed chain was designed according to the calculated transmission power as follows:

$$W_c = \frac{K_A W}{k_z} \quad [8]$$

where k_z is the tooth number coefficient.

Winnowing system

A brushless motor (type: Sunnysky; KV value: 1400; manufactured by Zhongshan Langyu Model Co., Ltd., China) was used as the fan, powered by the lithium battery (type: Geshi ACE 5C; capacity: 3300 mAh;

Table 2. Design parameters of conveyors.

Parameters	Values (mm)
Width of the belt of the input conveyor	200
Width of the belt of the output conveyor	280
Diameter of the driving wheel of the input conveyor	160
Diameter of the driving wheel of the output conveyor	224

manufactured by Shenzhen Grepow Battery Co., Ltd., China). The controller generated pulse width modulation waves to control the run and stop of the fan by controlling the electronic speed regulator (type: Skywalker 40A; manufactured by Shenzhen Hobbywing Technology Co., Ltd., China) and to adjust the airflow speed.

Control system

The circuit diagram of winnowing equipment is shown in Fig. 3. The type of central processing unit of controller (type: STM32-F103; manufactured by Guangzhou Hard Rock Technology Co., Ltd., China) was STM32-F103 ZET6, and its development environment was Keil uVision5. When machine-harvested *L. barbarum* entered the input conveyor, the fan started. The controller controlled the run and stop of electric motors by controlling the relays (type: SRD-05VDC-SL-C; manufactured by Ningbo Songle Relay Co., Ltd., China) and also adjusted the revolving speed of electric motors by controlling the electronic speed governors, so as to control the run and stop of the two conveyors and to adjust the input conveyor speed. The two conveyors rotated continuously to remove impurities such as unripe fruit, flowers, and leaves in machine-harvested *L. barbarum*.

DEM simulation of ripe fruit in the horizontal airflow

The horizontal airflow model was established based on C++ in Microsoft Visual Studio. Because the size of ripe fruit was approximately consistent and the horizontal airflow parameters (*e.g.*, velocity, density, and viscosity) were basically constant, the free flow resistance model was adopted (Hu, 2010). To accurately simulate the movement of ripe fruit in the horizontal airflow, its buoyancy and free flow resistance force should be considered (Liu *et al.*, 2015; Liu, 2018; Yu *et al.*, 2018). The equations [9-12] were referred to Hu (2010). The equations of the buoyancy F_B and the free flow resistance force F_d are as follows:

$$F_B = \rho g V \quad [9]$$

$$F_d = 0.5\rho A|v|vC_D \quad [10]$$

where F_B is the buoyancy, N; F_d is the free flow resistance force, N; g is the gravitational acceleration, m/s^2; V is the volume of ripe fruit, m^3; A is the projected area of ripe fruit perpendicular to the horizontal airflow

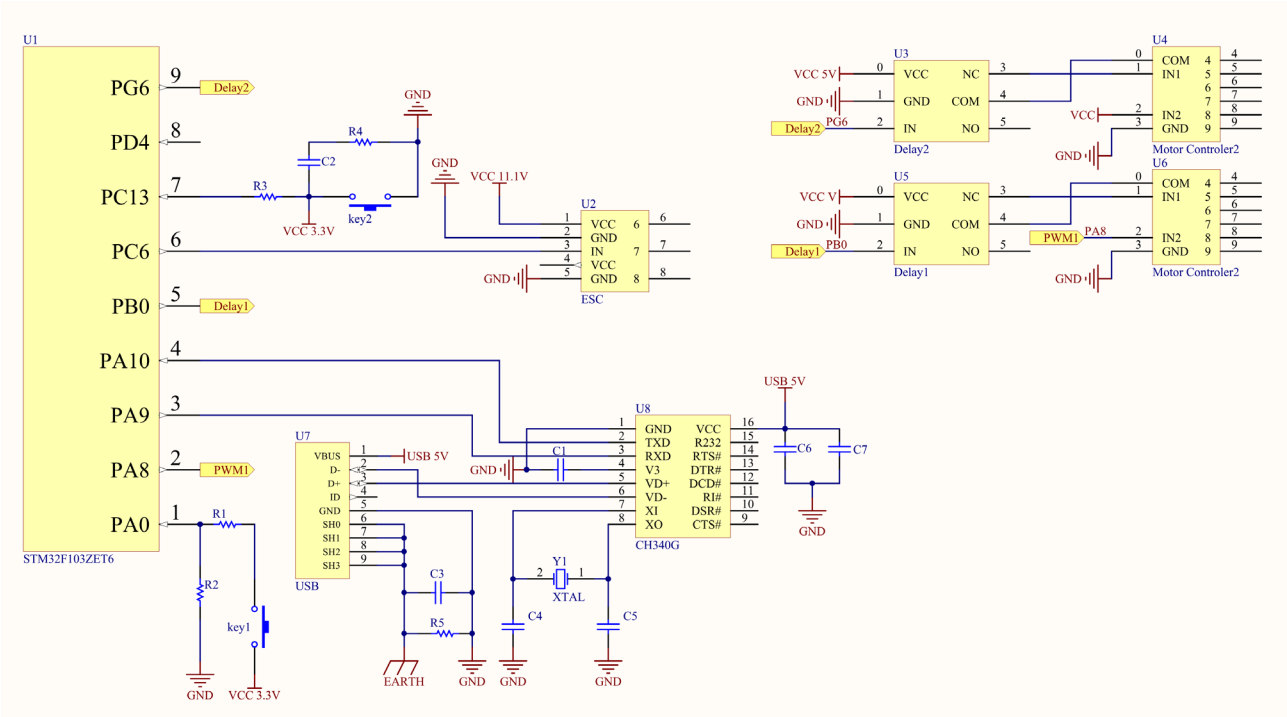

Figure 3. Circuit diagram of winnowing equipment.

direction, m²; v is the relative velocity between the ripe fruit and horizontal airflow, m/s; and C_D is the resistance coefficient which is calculated as follows:

$$C_D = \begin{cases} \dfrac{24}{Re} & Re \le 0.5 \\ \dfrac{24\left(1+0.25Re^{0.687}\right)}{Re} & 0.5 < Re \le 1000 \\ 0.44 & Re > 1000 \end{cases} \quad [11]$$

Therefore, C_D depends on the Reynolds number Re, and its equation is as follows:

$$Re = \frac{\beta \rho L |v|}{\eta} \quad [12]$$

where Re is the Reynolds number; β is the free volume of a grid cell; L is the diameter of ripe fruit, m; and η is the viscosity of horizontal airflow, kg/(m·s).

The movement of ripe fruit in the horizontal airflow was simulated based on DEM using EDEM software. In this study, the Moving Plane model was selected; the parameters of materials are listed in Table 1.

Based on previous research and references review (González-Montellano *et al.*, 2012; Horabik & Molenda, 2016; Castillo-Ruiz *et al.*, 2018; Chen *et al.*, 2019; Zhao *et al.*, 2019a,b), because the properties of *L. barbarum* are similar to the olives, some simulation parameters of olive can be cited based on the actual situation. Based on González-Montellano *et al.'s* (2012) work, because ripe fruit were distributed dispersedly with less collision compared with the olives, the restitution coefficient between ripe fruit and ripe fruit and the same coefficient between ripe fruit and the input conveyor were 0.1 and 0.1, respectively. Based on the reference (González-Montellano *et al.*, 2012), because there are irregular bulges on partial surfaces of ripe fruit and the mechanics parameters of the two conveyors material were listed in Table 1, the static friction coefficient between ripe fruit and the input conveyor was 0.5. Besides, the friction force between ripe fruit and ripe fruit was less than the friction force between ripe fruit and the input conveyor, the static friction coefficient between ripe fruit and ripe fruit was 0.3. Based on references review (Li *et al.*, 2012; Liu, 2018), the rolling friction coefficient between ripe fruit and ripe fruit and the same coefficient between ripe fruit and the input conveyor were select as the default value (*i.e.*, 0.01). Because the mass of ripe fruit is not very light and ripe fruit were distributed dispersedly, the movement of ripe fruit in the horizontal airflow was mainly affected by the gravity, horizontal airflow force, buoyancy, and free flow resistance force. Based on the pre-simulation, we came to a conclusion that the six coefficients have little effect on the simulation results. Therefore, the six coefficients were appropriate for this simulation. Furthermore, the ripe fruit model used a sphere with a radius of 4.5 mm. A 4-edged polygon served as the particle factory surface, and the type of particle factory was unlimited quantity. The DEM simulation of ripe fruit in the horizontal airflow is shown in Fig. 4.

According to the simulation, the airflow speed, input conveyor speed, and input-output conveyor distance greatly affected the rate of impurity change and the clearance rate of ripe fruit. Simulation results showed that winnowing equipment met these conditions, with most of ripe fruit falling on the output conveyor and most of unripe fruit, flowers, and leaves removed at an airflow speed of 5-6 m/s, input conveyor speed of 0.4-0.6 m/s, and input-output conveyor distance of 260-270 mm. Fig. 5 shows the trajectory of the ripe fruit which was the most easily removed by mistake.

Performance experiment of winnowing equipment

Ningqi 7 was selected as the experiment variety. The following instruments were used: 1) an electronic vernier caliper (type: AIRAJ second-generation product; range: 0-300 mm; precision: 0.01 mm; manufactured by Qingdao Yigou Hardware Tools Co., Ltd., China); 2) a digital illuminometer (type: PM6612L; manufactured by Shenzhen New Huayi Instrument Co., Ltd., China); 3) a tachometer (type: DT2236B; manufactured by Shenzhen Sanpo Instrument Co., Ltd., China); 4) a digital anemometer (type: PM6252B; manufactured by Shenzhen New Huayi Instrument Co., Ltd., China).

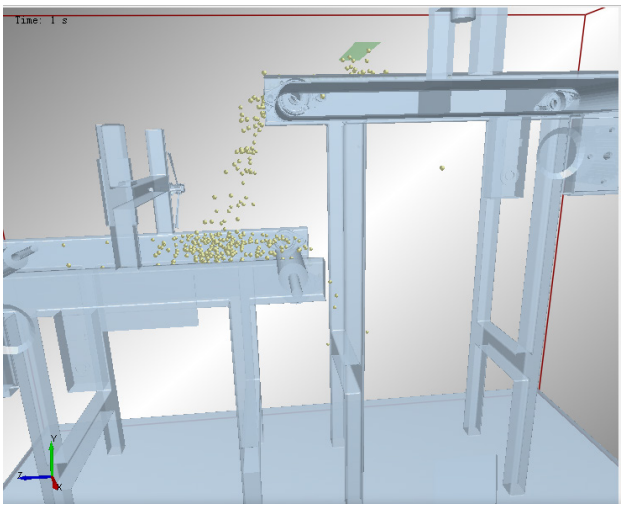

Figure 4. DEM simulation of ripe fruit in the horizontal airflow.

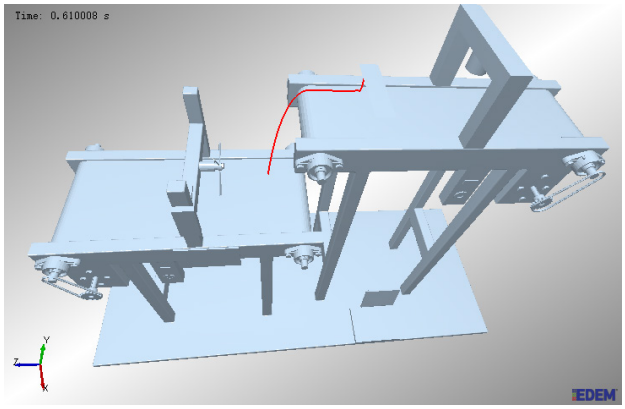

Figure 5. Trajectory of the ripe fruit.

The winnowing equipment was used to remove as many impurities as possible (*e.g.*, unripe fruit, flowers, and leaves) in machine-harvested *L. barbarum* while removing as little ripe fruit as possible. The purpose of the experiment was to investigate the performance of the winnowing equipment; therefore, the rate of impurity change Y_1 and the clearance rate of ripe fruit Y_2 were selected as performance indices in the experiment. Corresponding equations to calculate these indices are as follows:

$$Y_1 = \frac{\frac{n_1}{n_2} - \frac{n_3}{n_4}}{\frac{n_1}{n_2}} \times 100\% \quad [13]$$

$$Y_2 = \frac{n_5}{n_6} \times 100\% \quad [14]$$

where n_1 is the amount of unripe fruit, flowers, and leaves before winnowing; n_2 is the amount of ripe fruit, unripe fruit, flowers, and leaves before winnowing; n_3 is the amount of unripe fruit, flowers, and leaves after winnowing; n_4 is the amount of ripe fruit, unripe fruit, flowers, and leaves after winnowing; n_5 is the amount of removed ripe fruit after winnowing; and n_6 is the amount of ripe fruit before winnowing.

The experiment was conducted in Zhongning in the Ningxia Hui Autonomous Region (37°22′56″N, 105°37′21″E) on June 26, 2018; the temperature was 27.2°C, the humidity was 30.1%, and the illuminance was 520.6 Lux. Based on the theoretical analysis, the main factors affecting the performance of the winnowing equipment were determined to be the airflow speed, input conveyor speed, and input-output conveyor distance. The previous tests and simulation analysis indicated the following suitable value range for the factors: the airflow speed X_1 was 5-6 m/s; the input conveyor speed X_2 was 0.4-0.6 m/s; and the input-output conveyor distance X_3 was 260-270 mm. The airflow speed was adjusted by the electronic speed regulator and measured with the digital anemometer. The input conveyor speed was adjusted by the electronic speed governor and measured with the tachometer. The input-output conveyor distance was adjusted by lifting the input conveyor and measured with the electronic vernier caliper.

Three factors and three levels were used in a quadratic orthogonal rotation design; the codes of factors are listed in Table 3, and the experimental schemes and results are presented in Table 4. Seventeen groups of tests were carried out in this experiment, and each group was repeated 5 times. The mean value of 5 results was used as the group result. The machine-harvested *L. barbarum* from a shrub using a handheld *L. barbarum* harvester was used as a group sample. The amounts of ripe fruit, unripe fruit, flowers and leaves were manually counted before a test and the amounts of that were also manually counted after a test. Experiment design and analysis were performed in Design-Expert (Yuan *et al.*, 2012; Wang *et al.*, 2013).

Results

Regression analysis

The regression model of the rate of impurity change (response) using codes of all factors as variables was as follows:

$$Y_1 = 90.04 + 0.61X_1 + 0.27X_2 + 0.24X_3 - 0.095X_1X_2 + \\ + 0.04X_1X_3 + 0.025X_2X_3 - 1.24X_1^2 - 0.7X_2^2 - 0.68X_3^2 \quad [15]$$

ANOVA results of the rate of impurity change are shown in Table 5. The model was statistically significant (p<0.0001), and X_1, X_2, X_3, X_1X_2, X_1^2, X_2^2, and X_3^2 each had a significant effect on the rate of impurity change (p<0.05). Moreover, the lack-of-fit test indicated that the model had a good fit (p=0.1569).

The regression model of the clearance rate of ripe fruit (response) using codes of all factors as variables was as follows:

Table 3. Codes of factors.

Codes	Airflow speed (m/s)	Input conveyor speed (m/s)	Input-output conveyor distance (mm)
-1	5	0.4	260
0	5.5	0.5	265
1	6	0.6	270

Table 4. Experimental schemes and results.

No.	Airflow speed (m/s)	Input conveyor speed (m/s)	Input-output conveyor distance (mm)	Rate of impurity change (%)	Clearance rate of ripe fruit (%)
1	-1	-1	0	87.21	10.07
2	1	-1	0	88.56	10.94
3	-1	1	0	87.82	10.52
4	1	1	0	88.79	11.72
5	-1	0	-1	87.28	10.11
6	1	0	-1	88.47	11.04
7	-1	0	1	87.69	10.48
8	1	0	1	89.04	11.45
9	0	-1	-1	88.14	10.55
10	0	1	-1	88.73	10.97
11	0	-1	1	88.54	11.05
12	0	1	1	89.23	11.52
13	0	0	0	90.04	8.49
14	0	0	0	89.96	8.51
15	0	0	0	90.07	8.46
16	0	0	0	90.03	8.57
17	0	0	0	90.12	8.52

$$Y_2 = 8.51 + 0.5X_1 + 0.27X_2 + 0.23X_3 + 0.082X_1X_2 + \\ + 0.01X_1X_3 + 0.012X_2X_3 + 1.02X_1^2 + 1.28X_2^2 + 1.24X_3^2 \quad [16]$$

ANOVA results of the clearance rate of ripe fruit are shown in Table 6. The model was statistically significant (p<0.0001), and X_1, X_2, X_3, X_1X_2, X_1^2, X_2^2, and X_3^2 each had a significant effect on the clearance rate of ripe fruit (p<0.05). Moreover, the lack-of-fit test indicated that the model had a good fit (p=0.0667).

Response surface analysis

The response surface methodology was used to analyze the effects of all factors on the rate of impurity change; the response surface results of the regression equation (Eq. [15]) are shown in Fig. 6. As shown in Table 5, the airflow speed, input conveyor speed, and input-output conveyor distance each had an extremely significant effect on the rate of impurity change. The

Table 5. ANOVA results of the rate of impurity change.

Items	Sum of squares	DF	Mean square	*F*-value	*p*-value
Model	15.65	9	1.74	271.95	<0.0001**
X_1	2.95	1	2.95	461.63	<0.0001**
X_2	0.56	1	0.56	87.84	<0.0001**
X_3	0.44	1	0.44	69.08	<0.0001**
X_1X_2	0.036	1	0.036	5.64	0.0492*
X_1X_3	0.0064	1	0.0064	1.00	0.3505
X_2X_3	0.0025	1	0.0025	0.39	0.5517
X_1^2	6.52	1	6.52	1019.62	<0.0001**
X_2^2	2.09	1	2.09	326.75	<0.0001**
X_3^2	1.94	1	1.94	303.97	<0.0001**
Residual	0.045	7	0.0064		
Lack-of-fit	0.031	3	0.010	3.02	0.1569
Pure error	0.014	4	0.0034		
Total	15.70	16			

DF: degree of freedom. *,**: the item is significant (p<0.05) or extremely significant (p<0.01), respectively.

Table 6. ANOVA results of the clearance rate of ripe fruit.

Items	Sum of squares	DF	Mean square	*F*-value	*p*-value
Model	22.75	9	2.53	524.00	<0.0001**
X_1	1.97	1	1.97	408.31	<0.0001**
X_2	0.56	1	0.56	116.44	<0.0001**
X_3	0.42	1	0.42	86.76	<0.0001**
X_1X_2	0.027	1	0.027	5.64	0.0492*
X_1X_3	0.0004	1	0.0004	0.083	0.7817
X_2X_3	0.0006	1	0.0006	0.13	0.7295
X_1^2	4.42	1	4.42	916.83	<0.0001**
X_2^2	6.87	1	6.87	1424.17	<0.0001**
X_3^2	6.42	1	6.42	1330.98	<0.0001**
Residual	0.034	7	0.0048		
Lack-of-fit	0.027	3	0.0091	5.49	0.0667
Pure error	0.0066	4	0.0017		
Total	22.79	16			

DF: degree of freedom.. *,**: the item is significant (p<0.05) or extremely significant (p<0.01), respectively.

interaction effect between the airflow speed and input conveyor speed was significant. As shown in Fig. 6a, as the airflow speed increased, the rate of impurity change first increased rapidly and then decreased slowly. As shown in Fig. 6b, as the input-output conveyor distance increased, the rate of impurity change first increased slowly and then decreased slowly. As shown in Fig. 6c, as the input conveyor speed increased, the rate of impurity change first increased slowly and then decreased slowly.

The response surface methodology was used to analyze the effects of all factors on the clearance rate of ripe fruit; the response surface results of the regression equation (Eq. [16]) are shown in Fig. 7. As shown in Table 6, the airflow speed, input conveyor speed, and input-output conveyor distance each had an extremely significant effect on the clearance rate of ripe fruit. The interaction effect between the airflow speed and input conveyor speed was significant. As shown in Fig. 7a, as the airflow speed increased, the clearance rate of ripe fruit first decreased lowly and then increased rapidly; in Fig. 7b, as the input-output conveyor distance increased, the clearance rate of ripe fruit first decreased rapidly and then increased rapidly; and in Fig. 7c, as the input conveyor speed increased, the clearance rate of ripe fruit first decreased rapidly and then increased rapidly.

After prediction, the optimal parameter combination was determined to be an airflow speed of 5.52 m/s, input conveyor speed of 0.5 m/s, and input-output conveyor distance of 265.04 mm.

Field experiment verification

The field experiment was completed on June 28, 2018 and 15 groups were conducted in this experiment to eliminate random errors. The chosen experiment parameter combination was an airflow speed of 5.52 m/s, input conveyor speed of 0.5 m/s, and input-output conveyor distance of 265.04 mm. As depicted in

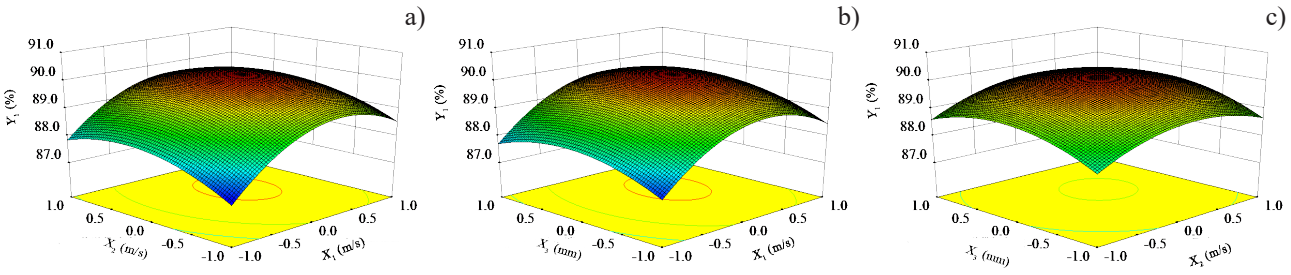

Figure 6. Response surface and contour plots for effects of all factors on the rate of impurity change: X_1 and X_2 (a), X_1 and X_3 (b), and X_2 and X_3 (c).

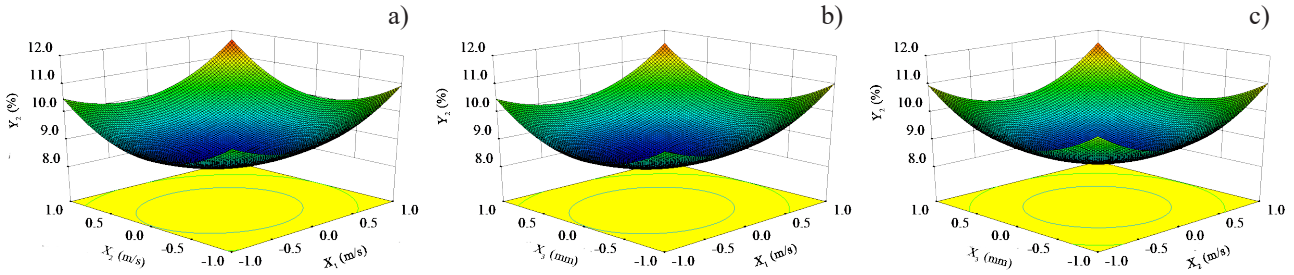

Figure 7. Response surface and contour plots for effects of all factors on the clearance rate of ripe fruit: X_1 and X_2 (a), X_1 and X_3 (b), and X_2 and X_3 (c).

Fig. 8, a high-speed camera (type: OLYMPUS i-speed TR; manufactured by Keymed (Medical & Industrial Equipment) Co., Ltd., UK) was used to record the winnowing process; the duration was 200 ms, the interval was 40 ms, and we used 1000 f/s (Torregrosa *et al.*, 2014; Liang *et al.*, 2018). Red, green, purple, and blue points were used to indicate the respective positions of the ripe fruit, unripe fruit, flower, and leaf every 40 ms. The field experiment showed that the rate of impurity change and the clearance rate of ripe fruit were 89.74% and 8.71%, respectively.

Discussion

The machine-harvested *L. barbarum* contained many impurities such as unripe fruit, flowers, and leaves (Zhang *et al.*, 2015; Wang, 2018; Xu *et al.*, 2018; Zhang *et al.*, 2018b; Chen *et al.*, 2019; Zhao *et al.*, 2019b). It seriously affected subsequent drying, storage, and other processing procedures. Therefore, it is important to develop winnowing equipment which can accurately and efficiently remove unripe fruit, flowers, leaves, and other impurities in machine-harvested *L. barbarum*. In the present study, winnowing equipment for machine-harvested *L. barbarum* based on the principle that different materials have different flight coefficients was designed. The structure and working parameters of winnowing equipment were optimized based on a DEM simulation and the field experiment. Moreover, we established mathematical models regarding the rate of impurity change and the clearance rate of ripe fruit based on the airflow speed, input conveyor speed, and input-output conveyor distance and analyzed the effects of all factors on the rate of impurity change and the clearance rate of ripe fruit. We came to a conclusion that the optimal parameter combination was an airflow speed of 5.52 m/s, input conveyor speed of 0.5 m/s, and input-output conveyor distance of 265.04 mm. The field experiment showed that the rate of impurity change

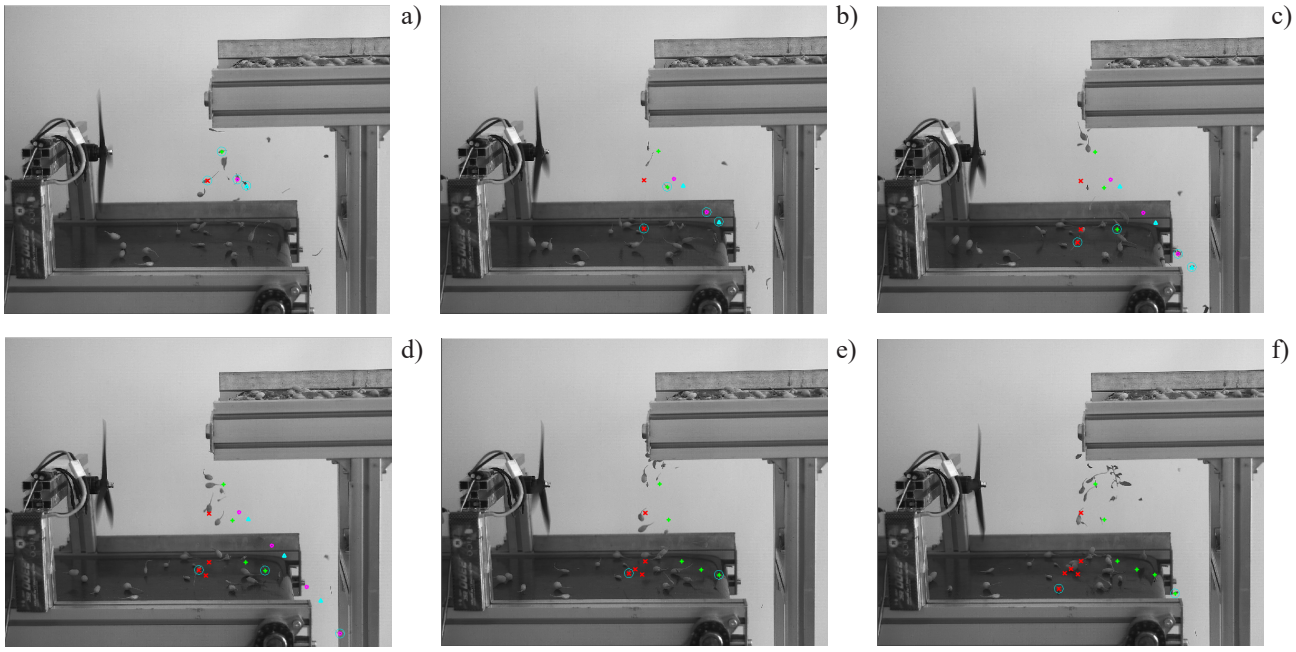

Figure 8. Winnowing process: 0 ms (a), 40 ms (b), 80 ms (c), 120 ms (d), 160 ms (e), and 200 ms (f).

and the clearance rate of ripe fruit were 89.74% and 8.71%, respectively. These results provide a design basis for future research on winnowing equipment for machine-harvested *L. barbarum*. But there are still some problems to be solved. For example, it is important to make miniaturized winnowing equipment, so as to real-time winnowing during harvesting. Furthermore, a more accurate and efficient winnowing method is also worth further studying.

References

Amagase H, Farnsworth NR, 2011. A review of botanical characteristics, phytochemistry, clinical relevance in efficacy and safety of *Lycium barbarum* fruit (Goji). Food Res Int 44 (7): 1702-1717. https://doi.org/10.1016/j.foodres.2011.03.027

Baidu WK, 2015. Elastic Modulus, Poisson's Ratio, and Density of Common Materials. https://wenku.baidu.com/view/6d0a67940b4e767f5acfcecf.html [19 May 2015].

Castillo-Ruiz FJ, Tombesi S, Farinelli D, 2018. Olive fruit detachment force against pulling and torsional stress. Span J Agric Res 16 (1): e0202. https://doi.org/10.5424/sjar/2018161-12269

Chen J, Zhao J, Chen Y, Bu LX, Hu GR, Zhang EY, 2019. Design and experiment on vibrating and comb brushing harvester for *Lycium barbarum*. T Chin Soc Agr Machin 50 (1): 152-161, http://dx.doi.org/10.6041/j.issn.1000-1298.2019.01.016

González-Montellano C, Fuentes JM, Ayuga-Téllez E, Ayuga F, 2012. Determination of the mechanical properties of maize grains and olives required for use in DEM simulations. J Food Eng 111 (4): 553-562. https://doi.org/10.1016/j.jfoodeng.2012.03.017

He M, Kan Z, Li CS, Wang LH, Yang LT, Wang Z, 2017. Mechanism analysis and experiment on vibration harvesting of wolfberry. T Chin Soc Agr Eng 33 (11): 47-53.

Horabik J, Molenda M, 2016. Parameters and contact models for DEM simulations of agricultural granular materials: A review. Biosyst Eng 147: 206-225. https://doi.org/10.1016/j.biosystemseng.2016.02.017

Hu GM, 2010. Analysis and simulation of granular system by discrete element method using EDEM: industrial application of discrete element method and EDEM software. Wuhan Univ Technol Press, Wuhan, China. 144 pp.

Li HC, Li YM, Gao F, Zhao Z, Xu LZ, 2012. CFD-DEM simulation of material motion in air-and-screen cleaning device. Comput Electr Agr 88: 111-119. https://doi.org/10.1016/j.compag.2012.07.006

Liang N, Ni FP, Zhang KL, Tang Y, Hu YH, 2018. Optimized installation angle and distance of a grading channel for dried jujube fruit with a push-pull actuating mechanism. Comput Electr Agr 150: 134-142. https://doi.org/10.1016/j.compag.2018.04.006

Liu FY, 2018. Discrete element modelling of the wheat particles and short straw in cleaning devices. Doctoral thesis. Northwest A&F Univ., Yangling, China.

Liu LY, Hao SY, Zhang M, Liu DM, Jia FG, Quan LZ, 2015. Numerical simulation and experiment on paddy ventilation resistance based on CFD-DEM. T Chin Soc Agr Machin 46 (8): 27-32+158.

Liu P, 2013. Research and design of large air classifier for high impurity raw grain. Master's thesis. Henan Univ. Technol., Zhengzhou, China.

Qiu XH, 2011. Machine design. Higher Education Press, Beijing, China. pp: 176-292.

So JD, 2001. Vibration characteristics of boxthorn (*Lycium chinense* Mill) branches. Appl Eng Agric 17 (6): 755-760. https://doi.org/10.13031/2013.6834

So JD, 2003. Vibratory harvesting machine for boxthorn (*Lycium chinense* Mill) berries. T ASAE 46 (2): 211-221. https://doi.org/10.13031/2013.12963

Torregrosa A, Albert F, Aleixos N, Ortiz C, Blasco J, 2014. Analysis of the detachment of citrus fruits by vibration using artificial vision. Biosyst Eng 119: 1-12. https://doi.org/10.1016/j.biosystemseng.2013.12.010

Wang CL, Peng HB, Ding J, Zhao BJ, Jia F, 2013. Optimization for vortex pump based on response surface method. T Chin Soc Agr Machin 44 (5): 59-65.

Wang YL, 2018. Research on key technology of wolfberry vibration harvest. Master's thesis. Northwest A&F Univ., Yangling, China.

Wang YL, Chen Y, Han B, Chen J, 2018. Research on laws of wolfberry dropping based on high-speed camera. J Agric Mechan Res 40 (11): 166-170.

Xu LM, Chen JW, Wu G, Yuan QC, Ma S, Yu CC, Duan ZZ, Xing JJ, Liu XD, 2018. Design and operating parameter optimization of comb brush vibratory harvesting device for wolfberry. T Chin Soc Agr Eng 34 (9): 75-82.

Yu LM, Xu Z, Yang JR, Fan WB, Li N, Long J, 2018. Numerical simulation of water and sediment movement in screen filter based on coupled CFD-DEM. T Chin Soc Agr Machin 49 (3): 303-308.

Yuan X, Qi LJ, Wang H, Huang SK, Ji RH, Zhang JH, 2012. Spraying parameters optimization of swing, automatic variables and greenhouse mist sprayer with response surface method. T Chin Soc Agr Machin 43 (4): 45-54.

Zhang WQ, Li ZZ, Tan YZ, Li W, 2018a. Optimal design and experiment on variable pacing combing brush picking device for *Lycium barbarum.* T Chin Soc Agr Machin 49 (8): 83-90.

Zhang WQ, Zhang MM, Zhang JX, Li W, 2018b. Design and experiment of vibrating wolfberry harvester. T Chin Soc Agr Machin 49 (7): 97-102.

Zhang Z, Xiao HR, Ding WQ, Mei S, 2015. Mechanism simulation analysis and prototype experiment of *Lycium*

barbarum harvest by vibration mode. T Chin Soc Agr Eng 31 (10): 20-28.

Zhao J, Sugirbay A, Chen Y, Zhang S, Liu FY, Bu LX, Chen Y, Wang ZW, Chen J, 2019a. FEM explicit dynamics simulation and NIR hyperspectral reflectance imaging for determination of impact bruises of *Lycium barbarum* L.. Postharvest Biol Technol 155: 102-110. https://doi.org/10.1016/j.postharvbio.2019.05.024

Zhao J, Chen Y, Wang YL, Chen J, 2019b. Experimental research on parameter optimization of portable vibrating and harvesting device of Chinese wolfberry. J Agric Mechan Res 41 (3): 176-182.

Zhao QH, Li JJ, Yan J, Liu S, Guo YL, Chen DJ, Luo Q, 2016. *Lycium barbarum* polysaccharides ameliorates renal injury and inflammatory reaction in alloxan-induced diabetic nephropathy rabbits. Life Sci 157: 82-90. https://doi.org/10.1016/j.lfs.2016.05.045

Zhou B, He J, 2010. Design of simulate hand wolfberry picking machine. T Chin Soc Agr Eng 26 (S1): 13-17.